J|A|C|S
ARTICLES
Published on Web 09/28/2006

Competition as a Design Concept: Polymorphism in Self-Assembled Monolayers of Biphenyl-Based Thiols

Piotr Cyganik,*,†,‡ Manfred Buck,*,† Thomas Strunskus,‡ Andrei Shaporenko,§ James D. E. T. Wilton-Ely,# Michael Zharnikov,§ and Christof Wöll‡

Contribution from the School of Chemistry, St Andrews University, North Haugh, St Andrews KY16 9ST, United Kingdom, Lehrstuhl für Physikalische Chemie I, Ruhr-Universität Bochum, Universitätsstrasse 150, 44801 Bochum, Germany, Angewandte Physikalische Chemie, Universität Heidelberg, Im Neuenheimer Feld 253, 69120 Heidelberg, Germany, and Chemistry Research Laboratory, University of Oxford, Mansfield Road, Oxford OX1 3TA, United Kingdom

Received June 9, 2006; E-mail: cyganik@if.uj.edu.pl; mb45@st-and.ac.uk

Abstract: Self-assembled monolayers (SAMs) of two ω-(4′-methylbiphenyl-4-yl)alkanethiols ($CH_3(C_6H_4)_2(CH_2)_nSH$, BP*n*, $n = 4, 6$) on Au(111) substrates, prepared from solution at room temperature and subsequently annealed at temperatures up to 493 K under a nitrogen atmosphere, were studied using scanning tunneling microscopy (STM), high-resolution X-ray photoelectron spectroscopy (HRXPS), and near-edge X-ray absorption fine structure spectroscopy (NEXAFS). In striking contrast to BP*n* SAMs with $n =$ odd, for which only one phase is observed, the even-numbered BP*n* SAMs exhibit polymorphism. Irreversible phase transitions occur which involve three phases differing substantially in density and stability. Upon annealing, BP4 and BP6 transform into a β-phase, which is characterized by an exceptionally high structural quality with virtually defect-free domains exceeding 500 nm in diameter. Exchange experiments, monitored by contact angle measurement, reveal that the β-phase exhibits a dramatically improved stability. The fundamental differences in the phase behavior of even- and odd-numbered BP*n* SAMs are discussed in terms of two design strategies based on cooperative and competitive effects.

I. Introduction

Self-assembled monolayers (SAMs) of thiols have played a crucial role in diverse areas of nanoscience for more than a decade. While the majority of work has concentrated on aliphatic systems,[1−3] the emerging field of molecular electronics and the efforts in lithography to address the ultrashort length scale have been major driving forces in the studies of SAMs of aromatic thiols.[4,5] Experiments performed in recent years have demonstrated that aromatic SAMs allow the control of charge transfer and the tailoring of electronic functionality[6−17] and offer new opportunities in lithography.[18−24]

One of the key issues facing nanotechnological applications of aromatic SAMs is the extent to which control over their structure and properties can be achieved. Since SAM structure is determined by a complex interplay of factors such as intermolecular interactions, molecule−substrate bonding, and mismatch between the lattices of SAM and substrate, a rational design of SAMs requires precise knowledge of these factors and their relative importance. While purely aromatic thiols[25−30] yield SAMs of fairly low structural quality, significantly lower than that of well-known aliphatic systems, the introduction of

† St Andrews University.
‡ Ruhr-Universität Bochum.
§ Universität Heidelberg.
# University of Oxford.

(1) Schreiber, F. *Prog. Surf. Sci.* **2000**, *65*, 151−256.
(2) Schwartz, D. K. *Annu. Rev. Phys. Chem.* **2001**, *52*, 107−137.
(3) Schreiber, F. *J. Phys.: Condens. Matter* **2004**, *16*, R881−R900.
(4) Ulman, A. *Acc. Chem. Res.* **2001**, *34*, 855−863.
(5) Love, J. C.; Estroff, L. A.; Kriebel, J. K.; Nuzzo, R. G.; Whitesides, G. M. *Chem. Rev.* **2005**, *105*, 1103−1170.
(6) Tour, J. M. *Acc. Chem. Res.* **2000**, *33*, 791−804.
(7) Fan, F. R. F.; Yang, J. P.; Cai, L. T.; Price, D. W.; Dirk, S. M.; Kosynkin, D. V.; Yao, Y. X.; Rawlett, A. M.; Tour, J. M.; Bard, A. J. *J. Am. Chem. Soc.* **2002**, *124*, 5550−5560.
(8) Adams, D. M.; et al. *J. Phys. Chem. B* **2003**, *107*, 6668−6697.
(9) Sikes, H. D.; Smalley, J. F.; Dudek, S. P.; Cook, A. R.; Newton, M. D.; Chidsey, C. E. D.; Feldberg, S. W. *Science* **2001**, *291*, 1519−1523.
(10) Creager, S.; Yu, C. J.; Bamdad, C.; O'Connor, S.; MacLean, T.; Lam, E.; Chong, Y.; Olsen, G. T.; Luo, J. Y.; Gozin, M.; Kayyem, J. F. *J. Am. Chem. Soc.* **1999**, *121*, 1059−1064.
(11) Felgenhauer, T.; Rong, H. T.; Buck, M. *J. Electroanal. Chem.* **2003**, *550*, 309−319.
(12) Ishida, T.; Mizutani, W.; Aya, Y.; Ogiso, H.; Sasaki, S.; Tokumoto, H. *J. Phys. Chem. B* **2002**, *106*, 5886−5892.
(13) Heath, J. R.; Ratner, M. A. *Phys. Today* **2003**, *56*, 43−49.
(14) Joachim, C.; Ratner, M. A. *Nanotechnology* **2004**, *15*, 1065−1075.
(15) Smalley, J. F.; Sachs, S. B.; Chidsey, C. E. D.; Dudek, S. P.; Sikes, H. D.; Creager, S. E.; Yu, C. J.; Feldberg, S. W.; Newton, M. D. *J. Am. Chem. Soc.* **2004**, *126*, 14620−14630.
(16) Dameron, A. A.; Ciszek, J. W.; Tour, J. M.; Weiss, P. S. *J. Phys. Chem. B* **2004**, *108*, 16761−16767.
(17) Baunach, T.; Ivanova, V.; Kolb, D. M.; Boyen, H.-G.; Ziemann, P.; Buettner, M.; Oelhafen, P. *Adv. Mater.* **2004**, *16*, 2024−2028.
(18) Geyer, W.; Stadler, V.; Eck, W.; Zharnikov, M.; Gölzhäuser, A.; Grunze, M. *Appl. Phys. Lett.* **1999**, *75*, 2401−2403.
(19) Felgenhauer, T.; Yan, C.; Geyer, W.; Rong, H. T.; Gölzhäuser, A.; Buck, M. *Appl. Phys. Lett.* **2001**, *79*, 3323−3325.
(20) Eck, W.; Stadler, V.; Geyer, W.; Zharnikov, M.; Gölzhäuser, A.; Grunze, M. *Adv. Mater.* **2000**, *12*, 805−808.
(21) Gölzhäuser, A.; Eck, W.; Geyer, W.; Stadler, V.; Weimann, T.; Hinze, P.; Grunze, M. *Adv. Mater.* **2001**, *13*, 806−809.
(22) Zharnikov, M.; Grunze, M. *J. Vac. Sci. Technol. B* **2002**, *20*, 1793−1807.
(23) Thom, I.; Buck, M. *Surf. Sci.* **2005**, *581*, 33−46.
(24) Smith, R. K.; Lewis, P. A.; Weiss, P. S. *Prog. Surf. Sci.* **2004**, *75*, 1−68.
(25) Kang, J. F.; Ulman, A.; Liao, S.; Jordan, R.; Yang, G. H.; Liu, G. Y. *Langmuir* **2001**, *17*, 95−106.

10.1021/ja0640647 CCC: $33.50

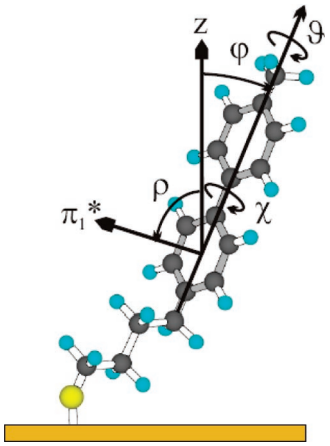

Figure 1. Structure of ω-(4′-methylbiphenyl-4-yl)butanethiol (BP4) and definition of coordinate system and angles for the biphenyl moiety. π_1* is perpendicular to the ring plane. χ refers to the dihedral angle of the phenyl rings.

an alkane spacer chain between the thiol headgroup and the aromatic moiety ($CH_3-(C_6H_4)_2-(CH_2)_n-SH$, BP*n*, $n > 1$; see Figure 1) results in high structural quality. This striking difference has been explained in terms of differences in the ways the systems can cope with misfit between the lattice of the aromatic moieties and the substrate lattice.[31] For the purely aromatic systems, the misfit giving rise to stress is predominantly resolved by introducing defects in the monolayer, i.e., domain boundaries, dislocation faults, or point defects.[30] In contrast, in the BP*n* systems[32−35] (characterized by the combination of aliphatic and aromatic moieties), additional degrees of freedom (e.g., conformational) are introduced, providing other pathways to reduce stress.

The pronounced improvement of film quality upon introduction of the alkane spacer is only one aspect. Another, less clear aspect is the striking influence of the number of methylene groups in the alkane spacer chain on the structure of the monolayers. Our previous spectroscopic[32,33] and microscopic[34,35] data have revealed that BP*n* SAMs exhibit a pronounced alternation in molecular orientation and coverage with the change between n = odd and n = even. This odd−even variation is also reflected in a number of properties of the BP*n* system, such as stability against exchange by other thiols[11] and electrochemical stability[23,36] as well as resistance to electron-induced modification of the film structure.[37] However, most striking for this class of SAMs is the odd−even difference upon annealing. While for n = odd only a gradual increase in film quality is observed but no obvious change in the molecular packing occurs, an unexpected phase transition is observed for the even-numbered BP4 system, resulting in a structure of significantly lower density. Besides a dramatic increase in the level of quality,[38] resulting in domains exceeding 10^5 nm^2, this phase transition causes a surprising increase in stability against exchange by other thiols when immersed in corresponding solutions. The phase transition seen for these biphenyl-based organothiolate adlayers is markedly different from the temperature-induced structural transitions into the low-density "flat-lying" phases known for alkanethiolate adlayers[39−44] with respect to both molecular orientation and stability.

Carrying on from our earlier communication, which reported the unexpected phase transition for BP4,[38] the present work represents an in-depth study of two BP*n* systems (BP4 and BP6), focusing on both the microscopic and spectroscopic details of their phase transitions. To do this, a combination of several complementary techniques, including scanning tunneling microscopy (STM), high-resolution X-ray photoelectron spectroscopy (HRXPS), and near-edge X-ray absorption fine structure spectroscopy (NEXAFS), has been employed. In addition, we performed exchange experiments and monitored them by water contact angle measurements.

II. Results

STM Experiments. Experimental details are given in the Supporting Information. Figures 2−5 summarize STM data obtained for BP4 and BP6 SAMs which were first prepared at room temperature from solution and subsequently annealed at different temperatures. Comparison of larger scale images, as presented in Figure 2a,d,g, Figure 4a,d,g, and Figure 5a, with respective STM data for samples prepared without annealing (see Figures 6c and 7c in ref 35 for direct comparison) shows a pronounced reduction in the density of substrate depressions (black islands in our STM data), characteristic for thiol adsorption on Au(111).[45−47] This well-known effect of thermally induced Ostwald ripening of these vacancy islands[48,49] is particularly striking here, as an essentially complete absorption of the vacancy islands into steps occurs even on extended terraces (Figures 2g and 4a). Another obvious feature already resolved at this large scale is a contrast variation seen as dark lines or extended areas such as the ones labeled β in Figure 2a. As detailed below, these contrast variations arise from structural transitions in the SAM. While the coexistence of different SAM structures is typical for intermediate temperatures, the contrast variations disappear at the high end of the temperature range investigated and over sufficiently extended annealing times, as documented by Figures 2g, 4g, and 5a.

(26) Leung, T. Y. B.; Schwartz, P.; Scoles, G.; Schreiber, F.; Ulman, A. *Surf. Sci.* **2000**, *458*, 34−52.
(27) Azzam, W.; Fuxen, C.; Birkner, A.; Rong, H. T.; Buck, M.; Wöll, C. *Langmuir* **2003**, *19*, 4958−4968.
(28) Yang, G. H.; Liu, G. Y. *J. Phys. Chem. B* **2003**, *107*, 8746−8759.
(29) Yang, G. H.; Qian, Y. L.; Engtrakul, C.; Sita, L. R.; Liu, G. Y. *J. Phys. Chem. B* **2000**, *104*, 9059−9062.
(30) Käfer, D.; Witte, G.; Cyganik, P.; Terfort, A.; Wöll, C. *J. Am. Chem. Soc.* **2006**, *128*, 1723−1732.
(31) Cyganik, P.; Buck, M.; Wilton-Ely, J. D. E. T.; Wöll, C. *J. Phys. Chem. B* **2005**, *109*, 10902−10908.
(32) Rong, H. T.; Frey, S.; Yang, Y. J.; Zharnikov, M.; Buck, M.; Wühn, M.; Wöll, C.; Helmchen, G. *Langmuir* **2001**, *17*, 1582−1593.
(33) Heister, K.; Rong, H. T.; Buck, M.; Zharnikov, M.; Grunze, M.; Johansson, L. S. O. *J. Phys. Chem. B* **2001**, *105*, 6888−6894.
(34) Azzam, W.; Cyganik, P.; Witte, G.; Buck, M.; Wöll, C. *Langmuir* **2003**, *19*, 8262−8270.
(35) Cyganik, P.; Buck, M.; Azzam, W.; Wöll, C. *J. Phys. Chem. B* **2004**, *108*, 4989−4969.
(36) Long, Y. T.; Rong, H. T.; Buck, M.; Grunze, M. *J. Electroanal. Chem.* **2002**, *524*, 62−67.
(37) Frey, S.; Rong, H. T.; Heister, K.; Yang, Y. J.; Buck, M.; Zharnikov, M. *Langmuir* **2002**, *18*, 3142−3150.
(38) Cyganik, P.; Buck, M. *J. Am. Chem. Soc.* **2004**, *126*, 5960−5961.
(39) Camillone, N.; Eisenberger, P.; Leung, T. Y. B.; Schwartz, P.; Scoles, G.; Poirier, G. E.; Tarlov, M. J. *J. Chem. Phys.* **1994**, *101*, 11031−11036.
(40) Poirier, G. E.; Pylant, E. D. *Science* **1996**, *272*, 1145−1148.
(41) Poirier, G. E. *Chem. Rev.* **1997**, *97*, 1117−1127.
(42) Staub, R.; Toerker, M.; Fritz, T.; Schmitz-Hubsch, T.; Sellam, F.; Leo, K. *Langmuir* **1998**, *14*, 6693−6698.
(43) Toerker, M.; Staub, R.; Fritz, T.; Schmitz-Hubsch, T.; Sellam, F.; Leo, K. *Surf. Sci.* **2000**, *445*, 100−108.
(44) Poirier, G. E.; Fitts, W. P.; White, J. M. *Langmuir* **2001**, *17*, 1176−1183.
(45) Edinger, K.; Gölzhäuser, A.; Demota, K.; Wöll, C.; Grunze, M. *Langmuir* **1993**, *9*, 4−8.
(46) Poirier, G. E. *Langmuir* **1997**, *13*, 2019−2026.
(47) Sondaghuethorst, J. A. M.; Schonenberger, C.; Fokkink, L. G. J. *J. Phys. Chem.* **1994**, *98*, 6826−6834.
(48) Poirier, G. E.; Tarlov, M. J. *J. Phys. Chem.* **1995**, *99*, 10966−10970.
(49) Cavalleri, O.; Hirstein, A.; Kern, K. *Surf. Sci.* **1995**, *340*, L960-L964.

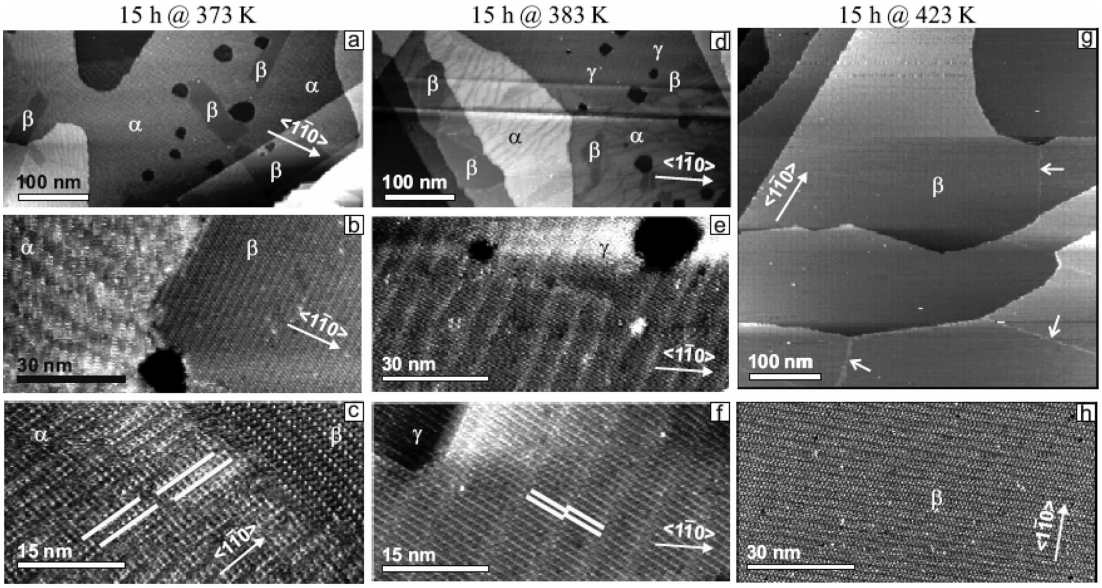

Figure 2. SAM of BP4 on Au(111). STM images at different resolutions showing samples prepared at room temperature and subsequently annealed in N_2 atmosphere for 15 h at 373 (a−c), 383 (d−f), and 423 K (g,h). α, β, and γ indicate areas covered by different phases as described in text. In (c) and (f), white lines indicate translational domains. In (g), arrows indicate domain boundaries.

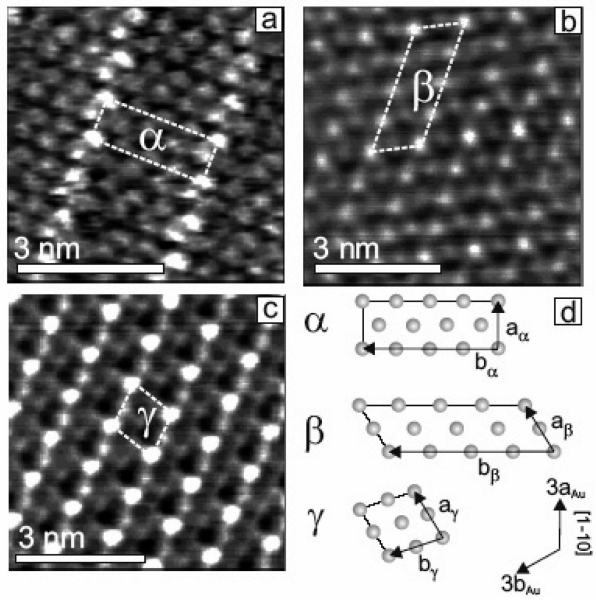

Figure 3. SAM of BP4 on Au(111). High-resolution STM images showing structure of the phases α (a), β (b), and γ (c). (d) Schematic drawing of the relative size, orientation, and molecular packing of unit cells $5\sqrt{3}\times3$, $6\sqrt{3}\times2\sqrt{3}$, and $2\sqrt{3}\times\sqrt{13}$, corresponding to α-, β-, and γ-phases, respectively.

Finally, a closer look at step edges reveals the occurrence of both the $\langle 1\bar{1}0\rangle$ directions, i.e., the one observed for the clean Au(111) substrate, and the $\langle 2\bar{1}\bar{1}\rangle$ directions. The latter can even come to dominate, as evidenced in Figure 4g for a BP6 SAM. It is also noted that the step edges along the $\langle 2\bar{1}\bar{1}\rangle$ directions correspond to the borderlines of the dark areas, and their emergence is associated with the structural transitions giving rise to the contrast.

To address in more detail the structural changes in BP4 and BP6 films upon annealing, we turn to high-resolution STM images, which allow the identification of single molecules. As has been demonstrated in our previous studies,[34,35] formation of the BP4 monolayer at room temperature results in the formation of a rectangular $5\sqrt{3}\times3$ structure with eight molecules per unit cell and an area per molecule of 27.05 Å^2. Details of this α-phase are presented in Figure 3. Data presented in Figure 2b,c show that annealing of a BP4 SAM at 373 K for 15 h creates areas where the α-phase transforms into an oblique $6\sqrt{3}\times2\sqrt{3}$ structure.[38] This β-phase also contains eight molecules per unit cell, but because the unit cell is significantly larger, the area per molecule increases to 32.4 Å^2 (Figure 3). Referring to Figure 2b,c we note that the β-phase formed during the annealing process exhibits a very high structural quality, whereas the neighboring α-phase is characterized by a mesh of translational domain boundaries separated by only about 10 nm (see markers in Figure 2c). A further increase in the structural complexity of the BP4 SAM is seen upon annealing for 15 h at a slightly higher temperature of 383 K. As shown in Figure 2d−f, an additional structure (γ-phase) emerges. This new structure can be described as an oblique $2\sqrt{3}\times\sqrt{13}$ structure with an area per molecule of 25.2 Å^2 (see Figure 3). The relationship between the unit cell vectors of the α, β, and γ structures ($\mathbf{a}_{\alpha,\beta,\gamma}$,$\mathbf{b}_{\alpha,\beta,\gamma}$) and the unit cell vectors of Au(111) ($\mathbf{a}_{Au}$,$\mathbf{b}_{Au}$) is quantitatively described by

$$\begin{pmatrix}\mathbf{a}_{\alpha,\beta,\gamma}\\ \mathbf{b}_{\alpha,\beta,\gamma}\end{pmatrix} = \mathbf{M}_{\alpha,\beta,\gamma}\begin{pmatrix}\mathbf{a}_{Au}\\ \mathbf{b}_{Au}\end{pmatrix} \quad (1)$$

where

$$\mathbf{M}_\alpha = \begin{pmatrix}3 & 0\\ 5 & 10\end{pmatrix};\quad \mathbf{M}_\beta = \begin{pmatrix}4 & 2\\ 6 & 12\end{pmatrix};\quad \mathbf{M}_\gamma = \begin{pmatrix}4 & 2\\ 1 & 4\end{pmatrix}$$

and graphically illustrated in Figure 3d.

The data presented in Figure 2d−f show that, in contrast to the β-phase, the γ-phase has a dense network of very regular translational domain boundaries. This is similar to the α-phase despite the differences in their regularity. Analysis of the STM data shows that the translational domain boundaries of the γ-phase run along the longer side of the oblique $2\sqrt{3}\times\sqrt{13}$ unit cell (vector $\mathbf{b}_\gamma$ in Figure 3d), i.e., along the $\langle 5\bar{1}\bar{4}\rangle$ directions.

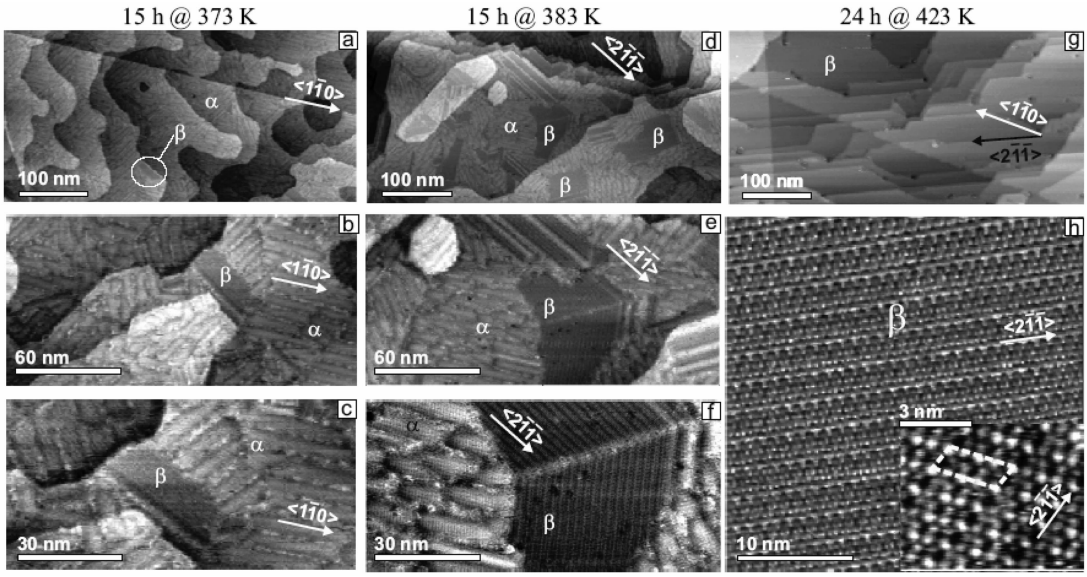

Figure 4. SAM of BP6 on Au(111). STM images at different resolutions showing samples prepared at room temperature and subsequently annealed in N_2 atmosphere at 373 K for 15 h (a−c), at 383 K for 15 h (d−f), and at 423 K for 24 h (g,h). α and β indicate areas covered by different phases as described in the text. Circled area in (a) marks the emergence of the β-phase. Inset in (h) shows high-resolution STM data of phase β with unit cell marked.

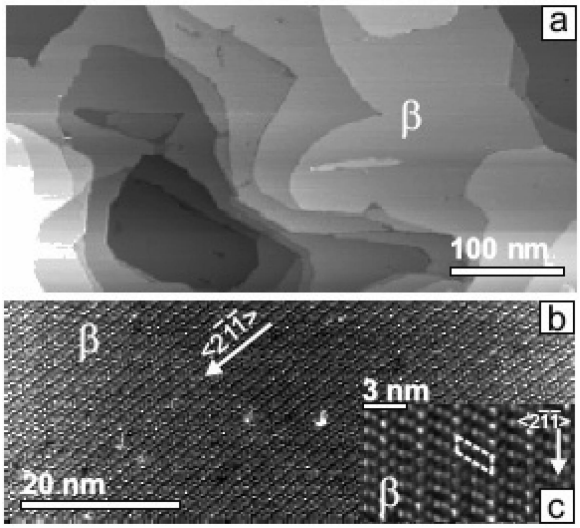

Figure 5. SAM of BP4 on Au(111). STM images at different resolutions (a−c) showing samples prepared at room temperature and subsequently annealed in N_2 atmosphere for 1.5 h at 493 K.

A final but important point to mention about the γ-phase is that this structure is temporary inasmuch as it only appears in addition to the other two phases. Upon further increase of the annealing temperature up to about 393 K (keeping the same annealing time of 15 h), this phase disappears, leaving only the α- and β-phases (data not shown). We note at this point that, since the γ-phase has domains in the nanometer range and was only observed together with the other two phases, this phase could only be identified by STM; a spectroscopic investigation with XPS or NEXAFS was impossible. For this reason, the structural model presented for this γ-phase is somewhat more tentative than those for the two other phases, α and β. On further increase of the annealing temperature, the fraction of the β-phase was found to increase at the expense of the α-phase. Finally, as demonstrated in Figure 2g,h, a complete transition to the β-phase can be obtained by annealing for 15 h at 423 K.

The structural quality, i.e., domain size and level of defects, of the β-phase at this point is exceptionally high. In this respect, it exceeds all other organothiol SAMs for which morphological data have been reported so far. Domains extending over 0.5 μm are routinely observed. Inspection of Figure 2 reveals that it is, in fact, quite difficult to locate defects (marked by arrows) within these ultrathin organic layers.

For BP6, an annealing behavior similar to that of BP4 is observed, as illustrated by the corresponding data of Figure 4. Our previous investigations[35] showed that this system exhibits the same $5\sqrt{3}\times3$ structure at low temperature as the BP4 system. In an analogous manner to the BP4 system, annealing at 373 K for 15 h also causes a new phase, seen as dark areas in Figure 4a−c, to appear. Analysis of the STM data yields the same oblique $6\sqrt{3}\times2\sqrt{3}$ structure as that observed for the β-phase reported above for the BP4 system (see data presented in Figure 4h). As found in the BP4 system, the quality of the β-phase is significantly higher than that of the coexisting α-phase, showing narrow, rectangular domains with the long axis along the ⟨110⟩ directions. This anisotropy has also been reported[35] in our previous experiments for the BP6 samples prepared from solutions at elevated temperature.

It is worth noting that the rectangular domains exhibit a symmetry which is different from the threefold symmetry of the Au(111) substrate. This implies the presence of three different rotational domains; the boundaries between these different rotational domains will, of course, contain a large number of defects. The only way to avoid such defects would be to use a substrate with two-dimensional symmetry.[50]

Increasing the annealing temperature to 393 K (with the same annealing time of 15 h) results in an increase of the area of the β-phase. A temperature of 423 K and an annealing time of 24 h are sufficient for a complete transition to the β-phase. The formation of the β-phase is accompanied by the pronounced formation of step edges along the $\langle 2\bar{1}\bar{1}\rangle$ directions. While BP6 and BP4 SAMs are very similar with respect to their α- and

(50) Lukas, S.; Witte, G.; Wöll, C. *Phys. Rev. Lett.* **2002**, *88*, 028301−028304.

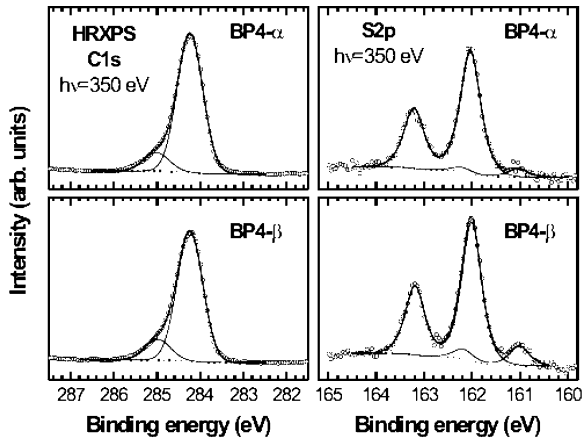

Figure 6. Normalized C 1s (left panels) and S 2p (right panels) HRXPS spectra of α-BP4/Au (upper panels) and *β*-BP4/Au (bottom panels) acquired at a photon energy of 350 eV. The spectra are decomposed into individual emissions or doublets (see text for details).

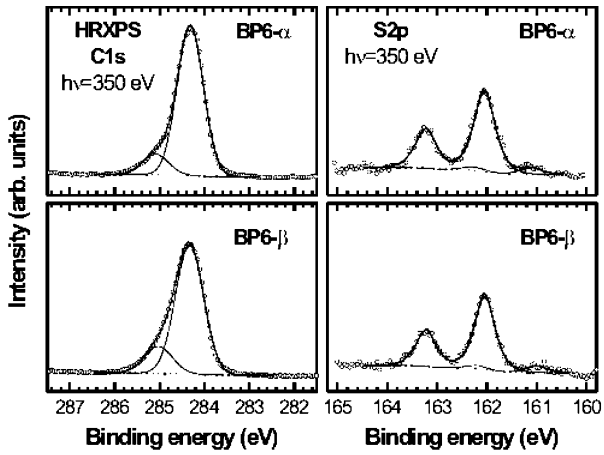

Figure 7. Normalized C 1s (left panels) and S 2p (right panels) HRXPS spectra of α-BP6/Au (upper panels) and *β*-BP6/Au (bottom panels) acquired at photon energy of 350 eV. The spectra are decomposed into individual emissions or doublets (see text for details).

β-phases, they are very different with regard to the *γ*-phase, which over the whole temperature range studied was only observed for BP4 but not for BP6.

To conclude this section, we note that even prolonged immersion of BP*n* SAMs exhibiting the *β*-phase in solutions of the respective BP*n* under conditions where the α-phase forms on a clean Au substrate does not lead to any significant structural changes. This suggests that the *β*-phase is either thermodynamically more stable than the α-phase also at room temperature or that the transition from the low-coverage *β*-phase to the higher-coverage α-phase is severely kinetically hindered (see discussion below).

The transition from the α- to the *β*-phase is determined by both temperature and annealing time. This is demonstrated by the data presented in Figure 5a−c. As shown, the full α→*β* transition in the BP4 system can be performed 10 times faster (1.5 h instead of 15 h) by increasing the corresponding annealing temperature from 423 to 493 K. However, with increasing temperature, time becomes more and more critical as the desorption channel becomes increasingly available.

HRXPS Experiments. Experimental details are given in the Supporting Information. The S 2p and C 1s HRXPS spectra of the α- and *β*-phases of BP4/Au(111) and BP6/Au(111) are presented in Figures 6 and 7, respectively. The spectra are normalized to the intensity of the incident X-ray beam and the number of scans so that a direct comparison between the individual spectra in the same spectral range is possible. The results of a quantitative analysis of the presented spectra are compiled in Table 1.

The S 2p HRXPS spectra are dominated by the S $2p_{3/2,1/2}$ doublet at a binding energy (BE) of ∼162.00 eV (S $2p_{3/2}$), commonly assigned to the thiolate species,[51] with no evidence for disulfides, alkylsulfides, or oxidative products. However, there is also a weak signal at ∼161 eV whose origin is not understood at present. This feature has been repeatedly observed for other thiol SAMs and two different assignments have been suggested,[52] either to atomic sulfur or to a thiolate species different from the majority thiolate species in the SAM. The presence of atomic sulfur as a result of decomposition during film preparation seems very unlikely here, as there is no indication of any decomposition from the other characterization techniques employed. In addition, the absence of any oxygen signal in XPS strongly suggests that the layer remains intact. Furthermore, as discussed below, the change in film thickness upon phase transition is also not compatible with a partial decomposition of the SAM. Since a change in hybridization of the S-atom orbitals can give rise to a core-level shift[53] and, as discussed in more detail below, the molecules used here must have a different bonding geometry from normal thiols, the second possibility appears most likely. However, the full details remain to be established.

For BP6 (Figure 7), the situation is essentially identical to that for BP4 except that the intensities are smaller due to a larger attenuation of the S 2p signal by the thicker BP6 films. The full width at half-maximum of the S $2p_{3/2,1/2}$ components is quite small for both BP4/Au(111) and BP6/Au(111), 0.50 and 0.48 eV for the α- and *β*-phases, respectively, indicating the high quality of the films.

The C 1s HRXPS spectra of the α- and *β*-phases of BP4/Au(111) and BP6/Au(111) also look very similar. The C 1s spectra show a main emission peak at a BE of 284.1−284.2 eV, assigned to the aromatic backbone, and a shoulder at ∼0.6 eV higher BE. Similar shoulders were observed previously for different aromatic SAMs and alternatively assigned to the carbon atom bonded to the sulfur headgroup or to shake-up processes.[33,54−57] The most recent HRXPS study of thiol-derived aromatic SAMs suggests that the former assignment is more likely.[52]

The intensity of the C 1s emission in the respective spectra in Figures 6 and 7 is not fully representative of the thickness of the corresponding films due to the saturation effect at this

(51) Heister, K.; Zharnikov, M.; Grunze, M.; Johansson, L. S. O. *J. Phys. Chem. B* **2001**, *105*, 4058−4061.
(52) Shaporenko, A.; Terfort, A.; Grunze, M.; Zharnikov, M. *J. Electron Spectrosc. Relat. Phenom.* **2006**, *151*, 45−51.
(53) Ishida, T.; Mizutani, W.; Azehara, H.; Hokari, H.; Akiba, U.; Fujihira, M.; Kojima, I.; Tokumoto, H. *Appl. Surf. Sci.* **1999**, *145*, 439−444.
(54) Gölzhäuser, A.; Panov, S.; Mast, M.; Schertel, A.; Grunze, M.; Wöll, C. *Surf. Sci.* **1995**, *334*, 235−247.
(55) Whelan, C. M.; Barnes, C. J.; Walker, C. G. H.; Brown, N. M. D. *Surf. Sci.* **1999**, *425*, 195−211.
(56) Whelan, C. M.; Smyth, M. R.; Barnes, C. J. *Langmuir* **1999**, *15*, 116−126.
(57) Frey, S.; Stadler, V.; Heister, K.; Eck, W.; Zharnikov, M.; Grunze, M.; Zeysing, B.; Terfort, A. *Langmuir* **2001**, *17*, 2408−2415.

Table 1. Summary of HRXPS Data for the BP4 and BP6 Films on Au(111) in the α- and β-Phases[a]

		BP4		BP6	
	peak	α-phase	β-phase	α-phase	β-phase
BE					
C1s	1	284.24 (0.70)	284.24 (0.70)	284.32 (0.69)	284.32 (0.74)
	2	285.02 (0.70)	285.00 (0.70)	285.09 (0.70)	285.03 (0.70)
S2p	1	162.03 (0.50)	162.01 (0.48)	162.05 (0.50)	162.04 (0.48)
	2	161.05 (0.50)	161.01 (0.48)	161.05 (0.50)	161.04 (0.48)
thickness (Å)		16.2	14.4	18.9	17.4

[a] Binding energy positions and the fwhm's (in parentheses) are in eV. For details of the thickness calculation, see text.

relatively low photon energy. Therefore, the thickness of the BP4 and BP6 films was evaluated on the basis of the Au 4f spectra and C 1s spectra acquired at a photon energy of 580 eV (not shown). A standard expression for an exponential attenuation of the photoemission signal was assumed.[58] The attenuation lengths of the C 1s (11.4 Å) and Au 4f photoelectrons (15.9 Å) were taken in accordance with the data reported by Lamont et al.[59] The derived film thicknesses (deviation ±0.7 Å) are presented in Table 1.

Comparison of the thickness values shows that the density of the α-phase is about 10% higher than that of the β-phase for both BP4 and BP6. While this difference in packing density is in qualitative agreement with the less dense packing seen for the β-phase in the STM experiments, this is lower than the 20% reduced density expected from the structural models shown in Figure 2, which yield an area per molecule of 27.05 Å^2 in the α-phase and 32.4 Å^2 in the β-phase. Considering this apparent discrepancy, one has to keep in mind that the densities derived from the structural model refer to perfectly ordered areas. The STM micrographs clearly demonstrate that the defect density is significantly larger for the α-phase than for the β-phase. As a result, the XPS thickness of the α-phase is expected to be somewhat reduced relative to that of the β-phase, which accounts for the apparent discrepancy.

NEXAFS Experiments. Experimental details are given in the Supporting Information. NEXAFS is a synchrotron-based spectroscopic tool to probe electric dipole transitions from core levels to unoccupied molecular orbitals close to the continuum.[60] The respective absorption resonances give a clear signature of a characteristic bond, a functional group, or a molecule. Moreover, since the cross section of the resonant photoexcitation process depends on the orientation of the electric field vector of the linearly polarized synchrotron light with respect to the molecular orbital of interest (so-called linear dichroism in X-ray absorption), information on molecular orientation can be derived from the experimental data.[60]

In Figure 8, C 1s NEXAFS spectra of the α- and β-phases for BP4/Au(111) and BP6/Au(111) acquired at 90° and 30° X-ray incidence angles are presented. The spectra exhibit characteristic absorption resonances due to the phenyl rings[57,61−63] (marked in the top part of Figure 8).

The most prominent is the π_1* resonance at ∼285.0 eV, which is accompanied by the weaker π_2* resonance at ∼288.9 eV, an R* resonance at ∼287.5 eV, and several broad σ* resonances

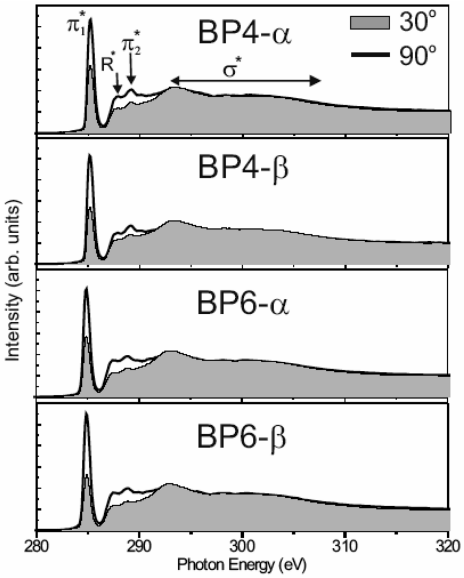

Figure 8. C 1s NEXAFS spectra for the α- and β-phases in the BP4/Au(111) and BP6/Au(111) samples acquired at X-ray incident angles of 90° and 30° (shadowed).

at higher photon energies. As is evident by the difference in the NEXAFS spectra taken at X-ray incidence angles of 90° and 30°, all investigated BP4 and BP6 samples exhibit a pronounced linear dichroism, which is a fingerprint of the orientational order. To determine the average tilt angles of the biphenyl backbones in the α- and β-phases of the BP4 and BP6 films, entire sets of the spectra acquired at different incidence angles were used. For this purpose, the intensity I of the most pronounced π_1* absorption resonance was monitored as a function of the X-ray incidence angle θ and evaluated according to the following theoretical expression (for vector-type orbital and substrate with threefold symmetry):[60]

$$I(\rho,\theta) \propto P\frac{1}{3}\left[1+\frac{1}{2}(3\cos^2\theta-1)(3\cos^2\rho-1)\right]+(1-P)\frac{1}{2}\sin^2\rho \quad (2)$$

where P denotes the polarization factor ($P \approx 82\%$), ρ as defined in Figure 1 corresponds to the angle of the transition dipole moment (TDM) for the transition in question relative to the surface normal, and the incidence angle θ of the X-ray beam is defined with respect to the surface plane. To avoid normalization

(58) Himmel, H. J.; Weiss, K.; Jäger, B.; Dannenberger, O.; Grunze, M.; Wöll, C. *Langmuir* **1997**, *13*, 4943−4947.
(59) Lamont, C. L. A.; Wilkes, J. *Langmuir* **1999**, *15*, 2037−2042.
(60) Stöhr, J. *NEXAFS Spectroscopy*; Springer-Verlag: Berlin, 1992.
(61) Fuxen, C.; Azzam, W.; Arnold, R.; Witte, G.; Terfort, A.; Wöll, C. *Langmuir* **2001**, *17*, 3689−3695.
(62) Azzam, W.; Wehner, B. I.; Fischer, R. A.; Terfort, A.; Wöll, C. *Langmuir* **2002**, *18*, 7766−7769.
(63) Hitchcock, A. P.; Fischer, P.; Gedanken, A.; Robin, M. B. *J. Phys. Chem.* **1987**, *91*, 531−540.

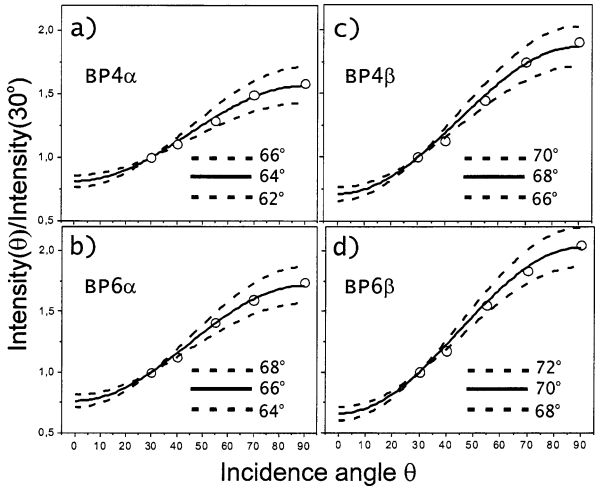

Figure 9. Angular dependence of the π_1* resonance intensity ratio, $I(\theta)/I(30°)$, for the BP4/Au(111) and BP6/Au(111) samples in the α- (a,b) and β-phases (c,d), respectively (θ denotes X-ray incidence angle). Data are presented together with the best theoretical fits (solid line). The values of the derived average TDM tilt angle (ρ) are given at the respective fits.

Table 2. Orientation of the Biphenyl Moiety Concluded from the NEXAFS Data for the BP4 and BP6 Films on Au(111) in the α- and β-Phases

	BP4		BP6	
	α-phase	β-phase	α-phase	β-phase
ρ	64°	68°	66°	70°
ϕ (for $\gamma = 32°$)[a]	31°	29°	26°	24°
ϕ (for $\gamma = 61°$)[b]	66°	58°	52°	45°

[a] Value taken from structure of the biphenyl crystal (see text for details). [b] Value taken from combined NEXAFS/IRRAS study (see text for details).

problems, intensity ratios $I(\rho,\theta)/I(\rho,30°)$ were analyzed. The experimental results, together with best fits based on eq 2, are presented in Figure 9 and summarized in Table 2. Average values of the angle ρ determined for the α-phases in the BP4 and BP6 films are 64° and 66°, respectively. The corresponding values for the β-phases in the BP4 and BP6 SAMs are 68° and 70°, respectively. Since the π_1* TDM is oriented perpendicular to the plane of the phenyl rings (see Figure 1), the value of the angle φ, corresponding to the tilt angle of the biphenyl moiety, is given by the following equation:

$$\sin \varphi = \frac{\cos \rho}{\cos \vartheta} \tag{3}$$

where ϑ is the twist angle of the coplanar biphenyl moiety around the 4,4′ axis ($\vartheta = 0$ for 4, 4′, *z*, and π_1* axes in one plane). Assuming a herringbone arrangement of the biphenyl moieties, which is typical for aromatic systems, and a twist angle ϑ as in bulk biphenyl[64] (32° [57,61,65,66]), φ values of 31° and 29° are obtained for the α-phases of BP4 and BP6, respectively. The corresponding φ values for the β-phase amount to 26° and 24°. However, from the combination of NEXAFS and IRRAS data in our previous study of the BP*n* ($n = 1-6$) homologues,[32]

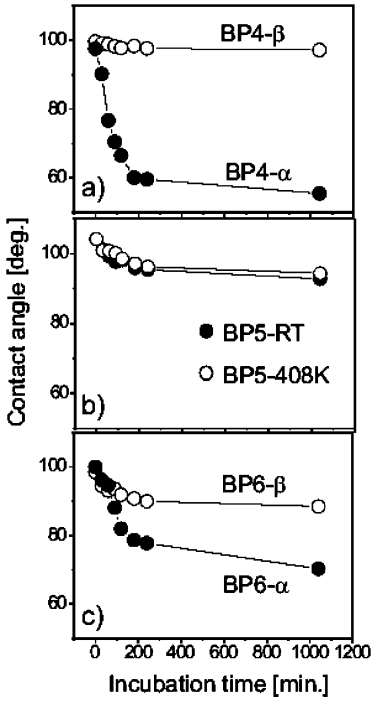

Figure 10. Contact angle measurements for the α- and β-phases in the BP4/Au(111) and BP6/Au(111) samples as a function of the incubation time in a 1 mM ethanolic solution of ω-mercaptohexadecanoic acid at room temperature (a,c). For comparison, in (b) are shown the corresponding data for the BP5/Au(111) sample prepared at room temperature and for the BP5/Au(111) sample prepared at room temperature and subsequently annealed at 408 K for 15 h.

a value of $\vartheta \approx 60°$ was estimated, for which φ values of about 66°/52° and 58°/45° are calculated for the α/β-phase of BP4 and BP6, respectively.

The NEXAFS results compiled in Table 2 yield a small but systematic increase of the π_1* TDM angle by $\Delta\rho \approx 4°$ for the α→β transition of both systems. With a fixed twist angle (ϑ) and using eq 3, this value can be transferred into a change in tilt angle φ. Data summarized in Table 2 show that, for $\vartheta \approx 32°$ ($\vartheta \approx 61°$), the tilt angle φ obtained for BP4 and BP6 in the β-phase is smaller by about 5° and 14°, respectively, compared to the α-phase. Since our STM and XPS data clearly show that the β-phase has lower packing density than the α-phase, one would expect an opposite change in the tilt angle, i.e., a higher value for the lower density β-phase. We take this discrepancy as an indication that the simplifying assumption of a phase-independent constant value of ϑ is not valid. We note at this point that in our recent systematic studies of terphenyl-substituted alkanethiols ($C_6H_5-(C_6H_4)_2-(CH_2)_n-SH$, TP*n*, $n = 1-6$),[65] a similar issue arose. From the inconsistency of NEXAFS and XPS/ellipsometry data, it was also concluded that the twist angle for the aromatic moiety in TP2 is markedly different from those in the rest of the TP*n* systems. A further point worth noting is that the dihedral angle χ (see Figure 1) between the phenyl rings in biphenyl is known to be very sensitive to its environment due to the relatively low energy barrier for rotation (about 62 meV/molecule).[67,68] Therefore, one can reasonably assume that the change in packing density by 20% upon the transition α→β is accompanied by a noticeable

(64) Charbonneau, G. P.; Delugeard, Y. *Acta Crystallogr.* **1976**, *B32*, 1420−1423.
(65) Shaporenko, A.; Brunnbauer, M.; Terfort, A.; Grunze, M.; Zharnikov, M. *J. Phys. Chem. B* **2004**, *108*, 14462−14469.
(66) Shaporenko, A.; Cyganik, P.; Buck, M.; Terfort, A.; Zharnikov, M. *J. Phys. Chem. B* **2005**, *109*, 13630−13638.
(67) Bastiansen, O.; Samdal, S. *J. Mol. Struct.* **1985**, *128*, 115−125.
(68) Brock, C. P.; Minton, R. P. *J. Am. Chem. Soc.* **1989**, *111*, 4586−4593.

change in the twist angle ϑ of the phenyl rings. However, it cannot be determined at present whether the measured twist angle changes are due to uniform changes of both phenyl rings and/or by change of the dihedral angle.

Exchange Experiments. Experimental details are given in the Supporting Information. To compare the relative stability of the α- and β-phases of BP4/Au(111) and BP6/Au(111) against exchange by other thiols, a series of contact angle measurements was performed. For this purpose, respective samples were incubated at room temperature in a 1 mM ethanolic solution of ω-mercaptohexadecanoic acid ($HS-(CH_2)_{15}-COOH$) for a given time, and then the drop in contact angle value (toward the value of about 50° obtained for ω-mercaptohexadecanoic acid SAMs formed by adsorption on clean Au) was used to monitor the exchange process. For comparison, the same type of experiment was also performed with BP5 SAMs. In this case, both samples prepared at room temperature and annealed at 408 K were investigated. Results obtained by this procedure are summarized in Figure 10. Data obtained for samples prepared at room temperature show a clear odd−even effect; i.e., the BP5 sample is significantly more stable against exchange of ω-mercaptohexadecanoic acid than the BP4 and BP6 samples. This observation is in agreement with previous IRRAS and electrochemical measurements of the exchange of BP*n* ($n = 1 - 6$) by hexadecanethiol, where a clear odd−even variation, i.e., a higher stability of the odd-numbered systems, was demonstrated.[11] Moreover, it was shown in this study that the stability of even-numbered systems against the exchange increases with the length of the aliphatic chain.[11] This effect is also visible in the exchange experiments presented here: the stability of the α-phase of BP6 is greater than that of BP4. Comparison of the exchange process for the α- and β-phases of the BP4 and BP6 samples shows that the α→β transition results in a pronounced improvement of the film in terms of stability against exchange by other thiols. Interestingly, annealing of the BP5 system, which leads to a substantial increase in the size of the domain structures but not to any phase transition, does not affect the exchange process. This indicates that the increase in film stability of even-numbered BP*n* SAMs upon annealing is not only related to the reduction in defect concentration due to growth of the domains, but also can be driven by the change in the film structure during the phase transition.

III. Discussion

The temperature-induced structural changes reported here for even-numbered BP*n* SAMs are distinctly different from those observed for other organothiolate adlayers on Au substrates. First, there is a striking contrast to the odd-numbered BP*n* homologues, which lack phase transitions. Second, the α→β phase transition is characterized by a pronounced increase in stability of the SAMs, even though the density is reduced by about 20%. This is in sharp contrast to phase transitions in alkanethiols,[39−44] where lower density phases, e.g., more tilted chains or molecules that lie flat, are not stable when immersed in solutions under conditions where a high-density phase forms.

The high stability of the low-coverage β-phase is, in fact, surprising since it is generally assumed that the rather strong

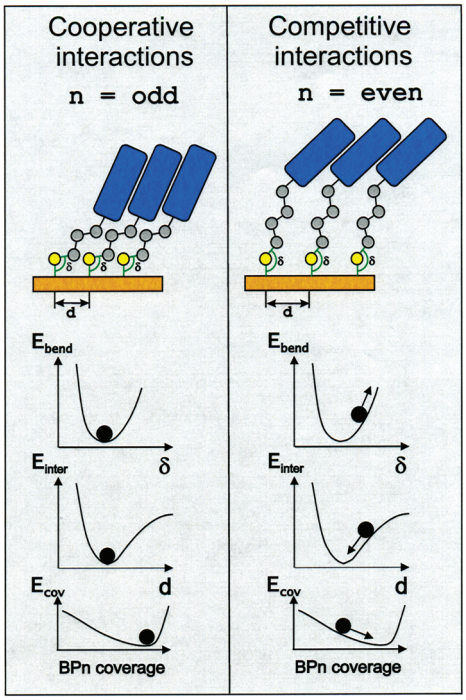

Figure 11. Schematic illustration of the cooperative and competitive way different energetic factors enter the energy balance in the n = odd and even BP*n* SAMs, respectively. E_{bend} corresponds to the energy associated with bending the Au−S−C bond (angle δ), E_{int} corresponds to the intermolecular interactions (d is the average distance between molecules), and E_{cov} corresponds to the coverage.

S−Au bond (with binding energies in the range of 1.6−2.0 eV/molecule[1,5,69]) is the major driving force for SAM formation and dominates any other contributions, e.g., from intermolecular interactions or conformational changes.

The surprising behavior of BP4 and BP6 raises a number of questions. What drives the phase transitions? Is it enthalpy or entropy, and to what extent are the formation and stability of the different phases determined by kinetics and/or thermodynamics?

To address these issues, we would like to start with an outline of the principal difference in the architecture of the systems presented here which gives rise to this unusual behavior. Referring to Figure 11, one can identify several factors which contribute to the energy balance of a SAM. For simplicity, they have been restricted to what we think are the most obvious ones, namely the Au−S bond density (or total coverage), molecule−molecule interactions, and the potential related to the bending of the Au−S−C bonds.[32,35,38] There are, of course, a number of additional contributions, such as the conformational degrees of freedom and/or the structure and energetics of the S−Au interface. The decisive point in this simple, qualitative model is that it depends on the molecular structure and whether the Au−S−C bending potential can be optimized at the expense of, or along with, other factors, such as the coverage, i.e., Au−S bond density and intermolecular interactions. For odd-numbered BP*n* SAMs and also alkanethiols, there is a strong driving force toward high coverage, as the energies of all three factors are driven toward a minimum and thus enter into the energy balance in a *cooperative* way. In contrast, for even-numbered BP*n* SAMs, the factors enter the energy balance in a *competitive*

(69) Ulman, A. *Chem. Rev.* **1996**, *96*, 1533−1554.

way; i.e., coverage and molecule−molecule interaction can only be optimized for an Au−S−C angle off the optimal value and vice versa. As a consequence, molecules of the cooperative type, such as odd-numbered BP*n*, form layers which are either in or close to a global minimum on the energy hypersurface. For alkanethiols which appear to be also of this type, there are only minor structural variations in the stable high-density phase; i.e., the density of the molecules is essentially unchanged.[70−73] In contrast, molecules of the competitive type, such as even-numbered BP*n*, yield SAMs of significantly higher energy and will, in general, have different structures with similar energies. For BP4 and BP6 SAMs, this results in the formation of the α-phase when prepared at lower temperature, whereas higher temperatures yield the less dense *β*-phase.

Two distinctly different models can be envisaged to explain the observed phase transitions. Model 1 assumes that the α-phase is the most stable; i.e., its formation is thermodynamically controlled. The α→*β* phase transition at elevated temperature is, in this case, entropy driven, as both desorption of molecules into the gas phase and a decrease in density of molecules in the SAM increase entropy. The observed stability of the *β*-phase is then a kinetic effect and is explained by the high structural quality of the *β*-phase, which makes insertion of molecules difficult and the reverse conversion to the higher density α-phase very slow.

In contrast, model 2 takes the opposite view and assumes that formation of the α-phase is kinetically controlled. In this case, heating provides the required activation energy for the irreversible transition from the metastable α-phase to the *β*-phase, which is lower in enthalpy and is thermodynamically more stable.

Which of the models actually applies cannot be unambiguously decided at present, since our knowledge of the energetics of the BP*n* phases and kinetics of the phase transitions is still too sparse. Nevertheless, we would like to address fundamental implications of the models and discuss the different experimental observations with respect to the effects of entropy and enthalpy.

Model 1 can provide a straightforward explanation for the phase transition from α to *β* upon annealing if one assumes that the *β*-phase is kinetically stabilized. Kinetic effects are well known in the formation and structural transition of thiol SAMs. Examples of this are the slow change of an octanethiol SAM from a c(4×2) to a $6\times\sqrt{3}$ structure[70] or the stepwise formation of alkanethiol SAMs,[74,75] which involves a fast step leading to a disordered adlayer with about 80% of the total coverage and subsequent steps in which the coverage increases only slightly but the orientational order develops. Strong kinetic hindrance is also observed when alkanethiolate SAMs are prepared by gas-phase deposition and when the coverage exceeds that of the striped phase.[76]

However, to explain the exchange data of the BP*n* SAMs (Figure 10), an exceptional kinetic stability of the *β*-phase has to be assumed. When the temperature-induced transition is complete, the *β*-phase is unusually stable with respect to exchange by other organothiols. This is demonstrated by the fact that the water contact angle changes upon immersion of a *β*-phase BP4 SAM into solutions of mercaptohexadecanoic acid by less than 2°, even for immersion times as long as 30 days. We have also not been able to achieve a conversion of the low-coverage *β*-phase back to the α-phase by re-immersion in the respective BP*n* solution under conditions where the α-phase forms on the clean Au substrate. Furthermore, prolonged immersion of a *β*-phase sample in alkanethiols results in an exchange (as observed in STM micrographs) only at domain boundaries and not inside ordered domains.

While the absence of the reverse conversion of phase *β* to phase α, at least on the time scale of our experiments, raises a question mark over the presence of kinetic limitations (model 1), model 2 requires introduction of an enthalpic contribution which favors the *β*-phase thermodynamically. The decrease in film density by 20% upon the α→*β* phase transition implies a significant difference in enthalpy, since the Au−S bond, which is characterized by binding energies in the range of 150−200 kJ/mol (1.6−2.0 eV/molecule),[1,5,70] is the major driving force for SAM formation. The fact that the lower density *β*-phase is not the one formed right away under standard preparative conditions makes it unlikely that an optimized Au−S−C bond angle (see Figure 11) at lower coverage is the driving force. Therefore, an additional enthalpic contribution is required.

One possibility centers on the interaction of the biphenyl moieties. In the α-phase their packing is energetically unfavorable, since it deviates substantially from the bulk structure of biphenyl. In the *β*-phase there has to be a significant relative shift of two biphenyl units along the 4,4′ axes and an improved interaction can be envisaged from geometrical considerations, i.e., the upper ring of one BP*n* molecule matching the lower ring of the neighboring molecule. Even though we cannot quantify the relative importance of the interaction of the biphenyl units, the change in twist angle upon phase transition, concluded from the NEXAFS data, is consistent with a sizable contribution of the biphenyl interaction. However, comparison of this contribution, which can be assumed to be well below the value of 0.2 eV/molecule for the enthalpy of fusion of biphenyl,[77] with the energy change associated with the decrease in coverage of about ∼0.3−0.4 eV/molecule due to the change in S−Au bond density, shows that other, more important contributions are required.

The only possibility left to provide significant gains in energy is the restructuring of the Au−S interface. For simple alkanethiols adsorbed on Cu(111)[78,79] and Ag(111),[80] a restructuring of the substrate has been reported. Also, in the case of Au(111), a significant restructuring has been suggested to explain the X-ray standing wave data for methane- and butanethiolate on Au(111).[81] Indirect evidence for a restructuring of the Au substrate upon α→*β* phase transformation comes from the observation

(70) Noh, J.; Hara, M. *Langmuir* **2002**, *18*, 1953−1956.
(71) Lüssem, B.; Müller-Meskamp, L.; Karthäuser, S.; Waser, R. *Langmuir* **2005**, *21*, 5256−5258.
(72) Fenter, P.; Eisenberger, P.; Liang, K. S. *Phys. Rev. Lett.* **1993**, *70*, 2447−2450.
(73) Pertsin, A. J.; Grunze, M. *Langmuir* **1994**, *10*, 3668−3674.
(74) Hähner, G.; Wöll, C.; Buck, M.; Grunze, M. *Langmuir* **1993**, *9*, 1955−1958.
(75) Himmelhaus, M.; Eisert, F.; Buck, M.; Grunze, M. *J. Phys. Chem. B* **2000**, *104*, 576−584.
(76) Himmel, H. J.; Wöll, C.; Gerlach, R.; Polanski, G.; Rubahn, H. G. *Langmuir* **1997**, *13*, 602−605.
(77) Chickos, J. S.; Hesse, D. G.; Liebman, J. F. *J. Org. Chem.* **1990**, *55*, 3833−3840.
(78) Parkinson, G. S.; Munoz-Marquez, M. A.; Quinn, P. D.; Gladys, M. J.; Woodruff, D. P.; Bailey, P.; Noakes, T. C. Q. *Surf. Sci.* **2005**, *598*, 209−217.
(79) Driver, S. M.; Woodruff, D. P. *Surf. Sci.* **2000**, *457*, 11−23.
(80) Yu, M.; Woodruff, D. P.; Bovet, N.; Satterley, C. J.; Lovelock, K.; Jones, R. G.; Dhanak, V. *J. Phys. Chem. B* **2006**, *110*, 2164−2170.
(81) Roper, M. G.; Skegg, M. P.; Fisher, C. J.; Lee, J. J.; Dhanak, V. R.; Woodruff, D. P.; Jones, R. G. *Chem. Phys. Lett.* **2004**, *389*, 87−91.

of major morphological changes. After the transition, monatomic steps are observed on the Au substrate which run along the $\langle 2\bar{1}\bar{1}\rangle$ directions. This is in pronounced contrast to clean Au(111) surfaces, where steps run predominantly along the $\langle 1\bar{1}0\rangle$ directions. Also, for organothiol SAMs, these steps are observed to run along the $\langle 1\bar{1}0\rangle$ directions. The increased number of steps running along $\langle 2\bar{1}\bar{1}\rangle$ is even more prominent for BP6, as can be seen in Figure 4g. We note that an area showing a high density of these steps was intentionally selected in order to demonstrate this effect. Since there are variations in step density across the sample, Figure 4g does not imply that the average step density is higher for BP6 compared to BP4.

Another indirect piece of evidence for structural changes at the Au−S interface comes from experiments investigating the effect of ion- and electron-induced desorption of aromatic SAMs. These show that Au−S bond scission strongly depends on the details of the Au−S interface[82] and where the $\alpha\rightarrow\beta$ transition significantly alters the fragmentation pattern, thus indicating pronounced changes in the relative strengths of the Au−S and S−C bonds.[83]

Finally, a restructuring at the S−Au interface is also supported by electronic structure calculations. Recent DFT studies have demonstrated that a thiol bound to an open gold surface is energetically more favorable than one bonded to the unreconstructed Au(111) surface.[84]

An important issue to be addressed with regard to the two models is the occurrence of the γ-phase. This phase cannot be prepared separately but always coexists with the α- and β-phases. The fact that the γ-phase exhibits the largest density of all phases ($\beta < \alpha < \gamma$) implies that the available area per molecule and the conformational space are smaller than those of the other phases and, accordingly, that the γ-phase is entropically least favorable. The higher density is also likely to result in a C−S−Au bond angle which differs more strongly from the optimum value than in the case of the other, lower density phases (see Figure 11). Since the C−S−Au bending potential contributes significantly to the total energy of the system (which, in fact, is the origin of the odd−even effect in BP*n* SAMs[32]), the enthalpy of the γ-phase will also be reduced. As a result of the entropic and energetic differences, the free energy of the γ-phase will be larger than those of the two other phases.

Assuming, for the moment, a structurally perfect α-phase and no desorption of molecules (see below), the expanded β-phase can only be formed from the α-phase if at the same time another, denser phase, the γ-phase, forms. Thus, an entropy-based explanation of the disproportionation of the α-phase into β- and γ-phases requires that the decrease in entropy upon formation of the γ-phase is overcompensated by the increase in entropy due to formation of the β-phase. In the enthalpy-based explanation of model 2, the lowering of the energy in the β-phase by restructuring of the interface, for example, compensates for the formation of the γ-phase with its higher enthalpy.

While in the ideal case the β- and γ-phases should form simultaneously from the α-phase, the β-phase always appears first in the experiment, and the γ-phase emerges only with progressive $\alpha\rightarrow\beta$ transformation. This behavior can be understood by taking into account the fact that the SAM is not perfect, and domain boundaries and other defects where the packing is less dense do exist. Therefore, at the onset of the $\alpha\rightarrow\beta$ phase transitions, the α-phase can expand to form the β-phase by using up this available space without forming the γ-phase. Only after consumption of this space does the medium-density α-phase disproportionate into the high- (γ) and low-density (β) phases. At sufficiently high temperatures, the entropically favorable desorption channel becomes available, which is required to eliminate the γ-phase and complete the $\alpha\rightarrow\beta$ transition. As a final remark on the γ-phase, we note that the conditions under which it appears depend on the particular BP*n*. In BP4 SAMs, the γ-phase is observed both upon annealing in a nitrogen atmosphere and upon preparation at elevated temperatures from solution (60 h at 363 K, data not shown), whereas in BP6 SAMs, it is only observed upon preparation from solution. The sensitivity of the detailed course of the phase transition to changes in the spacer from four to six methylene units reflects the complex interplay of factors governing the energetics and kinetics of the systems. It adds to the differences in the annealing behavior of the α-phase which, in contrast to BP4, exhibits a pronounced anisotropy of domains for BP6.[35]

A final point of interest concerning the relevance of the different models is the observation that the β-phase forms domains of size and quality which are unprecedented for aromatic-based SAMs. Furthermore, the STM images are perfectly uniform (Figure 1g) and do not show any height variations beyond the ones due to the molecular arrangement (Figure 1h). This is in contrast to the α-phase, which shows contrast variations on a length scale of a few nanometers as a sign of stress resulting from the mismatch between SAM and substrate lattices.[31,35] These observations are a clear indication that the β-phase is a structure which is low in stress. A change in energy associated with release of stress upon the $\alpha\rightarrow\beta$ phase transition is another force which can make a significant contribution to drive the transition. In contrast to the other observations, which can be explained by both models, the change in stress favors model 2.

IV. Conclusions

The experiments presented above, together with preceding experiments on BP*n* SAMs,[27,31,32,38,34,35] clearly demonstrate that control of structure and quality of a SAM requires careful tuning of the factors which determine the energy balance. The behavior of BP*n* SAMs reveals the presence of several important factors whose relative importance and mutual influence depend intimately on the molecular structure. Two principal strategies for tailoring SAMs can be adopted which differ in how the various factors, such as intermolecular interactions, coverage, and bonding configuration at the Au−S interface (see Figure 11), enter the energy balance. The first of these, which is usually pursued and applies also to BP*n* on Au with $n =$ odd, is based on cooperative effects; i.e., the molecular structure is chosen such that all relevant energy-determining factors can be optimized. This scenario will typically result in the presence of one structure which is significantly more stable than other structures with different types of molecular packing. The second strategy, which applies to BP*n* on Au with $n =$ even, is built on competitive effects. In this case, different factors such as molecular packing and Au−S−C bond angle cannot be opti-

(82) Cyganik, P.; Vandeweert, E.; Postawa, Z.; Bastiaansen, J.; Vervaecke, F.; Lievens, P.; Silverans, R. E.; Winograd, N. *J. Phys. Chem. B* **2005**, *109*, 5085−5094.
(83) Vervaecke, F. Ph.D. Thesis, Katholieke Universiteit Leuven, 2005.
(84) Molina, L. M.; Hammer, B. *Chem. Phys. Lett.* **2002**, *360*, 264−271.

mized at the same time. As a consequence, different structures with different types of molecular packing result which are similar in energy. These structures will differ in coverage and the molecular arrangement within the films. There are many SAMs of the cooperative type which yield only one stable, low-energy structure (or several very similar ones[71,70]) due to the match of factors such as Au−S−C bond angle and the intermolecular interactions.[85,32] However, it is more interesting to have a situation with several energetically closely spaced structures, opening up new opportunities in the design and application of SAMs.

A pleasing aspect associated with the phase transitions is the pronounced improvement in the structural quality. This is a quite distinct difference from other monolayer systems, e.g., SAMs[86] or metal-on-metal,[87] where competition between factors such as different lattices also plays a role but results in disorder or defect formation. Another advantage is that preparation under normal conditions, i.e., from solution at room temperature, results in a metastable structure which transforms into a more stable one upon annealing. This switch in stability might be exploited for lithographic applications.

With the experiments on BP4 and BP6 presented above, an essentially unexplored territory of the energy and structure landscapes of thiol self-assembled monolayers has been entered. To improve our fragmented knowledge about the phase behavior, a number of crucial issues have to be addressed, one of which is the kinetics of the phase transitions, i.e., the time scale−temperature relationship. Another goal is to elucidate the exact reason behind the improvement in structure upon transition to the β-phase. It is unclear to what extent the ability of this phase to cope with stress is due to an alteration in the intermolecular interactions by changing density or due to processes at the S−Au interface, such as restructuring. It is, in particular, the latter which we consider the key to understanding what is driving the phase transitions. This is the case since the energies involved in the restructuring of the thiol−substrate interface seem to be required to compensate for changes in the S−Au bond density and associated coverage-dependent factors which enter into the energy balance.

Acknowledgment. This work was supported by The Leverhulme Trust, German Science Foundation, EPSRC, and SHEFC. P.C. was a Postdoctoral Fellow of the Alexander von Humboldt Foundation. This work has been supported by the German BMBF (05KS4VHA/4) and European Community (Access to Research Infrastructure action of the Improving Human Potential Program).

Supporting Information Available: Complete ref 8 and experimental section. This material is available free of charge via the Internet at http://pubs.acs.org.

JA0640647

(85) Tao, Y. T.; Wu, C. C.; Eu, J. Y.; Lin, W. L. *Langmuir* **1997**, *13*, 4018−4023.
(86) Duan, L.; Garrett, S. J. *J. Phys. Chem. B* **2001**, *105*, 9812−9816.
(87) Jacobsen, J.; Nielsen, L. P.; Besenbacher, F.; Stensgaard, I.; Laegsgaard, E.; Rasmussen, T.; Jacobsen, K. W.; Norskov, J. K. *Phys. Rev. Lett.* **1995**, *75*, 489−492.